# *Carbon Nanoflakes and Carbon Nanowalls*

## *An innovation in Biosensors*

**Matthias Van Gompel**

promotor :
Prof. dr. Patrick WAGNER

co-promotor :
Prof. dr. Ken HAENEN

Eindverhandeling voorgedragen tot het bekomen van de graad master in de biomedische wetenschappen bio-elektronica en nanotechnologie

Universiteit Maastricht

universiteit hasselt

# Preface

Getting to this point, delivering a finished thesis, has been an interesting voyage, one which required a lot of work and the help of a lot of people.

First I would like to thank Rob Vansweevelt, for all the support he gave me and for proposing such an intriguing topic as this. He helped me when things became difficult, and with his infinite patience, put up with me for over six months.

I also want to thank my promotor, Patrick Wagner, for advising me when I needed it, and especially for all the interesting classes he gave while I studied for my Master's degree.

Without materials to do experiments with, research can be difficult, so thanks go to Alexander Malesevic from Vlaamse Instelling voor Technologisch Onderzoek, for growing the carbon nanowall samples.

Luckily, I came into an environment at the Institute for Material Research, where the colleagues from the BIOS group always made a very relaxing and entertaining atmosphere. Thanks, Lars, Evi, Jan, Bart, Rob and Bert.

Thanks also go to Kathe Grooms, for her technical editing.

Last, I would like to thank my parents and my sister for the support they gave me the last five years.

# Abbreviations

| | |
|---|---|
| CNF | Carbon nanoflakes |
| CNT | Carbon nanotubes |
| CNW | Carbon nanowalls |
| CVD | Chemical vapor deposition |
| DNA | Deoxyribonucleic acid |
| EDC | 1-ethyl-3-(3-dimethylaminopropyl)-carbodiimide |
| ELISA | Enzyme-linked immunosorbent assay |
| HOPG | Highly oriented pyrolytic graphite |
| MES | 2-[N-morpholino]-ethanesulphonic acid |
| MWPECVD | Micro wave plasma enhanced chemical vapor deposition |
| NCD | Nanocrystalline diamond |
| SAM | Self-assembled monolayer |
| SNP | Single nucleotide polymorphism |
| ssDNA | Single-stranded deoxyribonucleic acid |

# Abstract

Over the last couple of years, graphene and other related materials such as carbon nanowalls (CNWs) and carbon nanoflakes (CNFs) have become a very important research subject in microelectronics. The use of these two carbon-based materials in biosensor research is not yet explored. But carbon nanotubes (CNT), a related material, are already being pursued as a possible material to use in biosensors [1, 2, 3].

Carbon-based materials with SNP sensitivity have already been used to create ssDNA biosensors [4]. But the fabrication of nano crystalline diamond (NCD) is expensive, and not possible on a large scale, which will be a possibility for graphene and CNFs. The physical properties of CNWs and CNFs may make it possible to develop a more sensitive sensor that will require less ssDNA material and will produce more stable measurements.

In the first stage of the research, ssDNA was covalently bonded to the CNWs. Since CNWs and diamond are all made of carbon, the method developed by P. Christiaens was used [5]. By functionalizing the CNWs with 10-undecenoic acid using UV-light, $H_2N$ terminated ssDNA was attached by EDC-mediated chemistry. To verify the bonding between ssDNA and the CNWs, Alexa-488 labeled DNA was used.

Using fluorescence microscopy, the bonding of DNA to the CNWs was verified. To test selectivity, measurements comparing fluorescence intensity between hybridization with complementary ssDNA and one mismatch ssDNA were done. A significant difference between both was found, and SNP selectivity was thus achieved. The CNWs were able to go through ten cycles of hybridization, followed by denaturation. This shows the reusability of the sensor platform. The physical and chemical properties of the CNFs and CNWs were researched by Hall measurements, impedance spectroscopy and by Raman spectroscopy. A grid of electrodes was used to measure the electrical properties of CNFs. The CNFs exhibit very low resistance, in the order of 50 $\Omega$.

# Contents

# Chapter 1

# Introduction

In 1956 Leland Clark [6] invented the first biosensor, which detected glucose. It was the beginning of the rapidly developing field of bioelectronics which draws input from physics, chemistry, biology, medicine and biomedical sciences. Bioelectronics hasn't stopped with the invention of the Clark glucose sensor, however. Today scientists are searching for new, more sensitive biosensors which are implantable, fast, cheap and easy to use. So a cheap point-of-care device is essential for a successful commercial biosensor. In recent times, a new and exciting phenomenon is emerging, as predicted by Richard Feynman. At the meeting of the American Physical Society of 1959 at Caltech, he remarked, "There is plenty of room at the bottom." Since small sensors are more practical to work with and are much easier to implant, nanotechnology can provide new insights on how to produce better biosensors. And the benefits don't stop there: Since the biological materials used in biosensors and bio-electronics are in the order of nanometers or at the most micrometers, the coupling of these two fields is logical. In this thesis, a biosensor that detects DNA is developed with the help of novel materials that were discovered with the rise of nanotechnology.

## 1.1 Biosensors

A biosensor generally consists of three main parts: a detection layer, a transducer layer and a readout. The detection layer contains a biological component, e.g., immunoglobulines, enzymes, cells, and DNA [6, 7, 8, 9]. When it detects a protein, a matching DNA strand, or any other biological target molecule, the signal given from the biological detection layer has to be converted to a more convenient signal to process and to work with. This is done by the transducer layer. The two most common methods are electrical signals or visual signals, like fluorescent light in an ELISA or a color strip in a pregnancy test. Although fluorescent light or color strips are easy to interpret, they limit further analysis of the sensor's results. A transducer that translates the biological signal into an electrical signal

is desirable. The electrical measurement can then be transfered to a computer which can manipulate the data and translate it in a result that is easy to interpret. In Figure 1.1, a schematic representation is given for a basic biosensor.

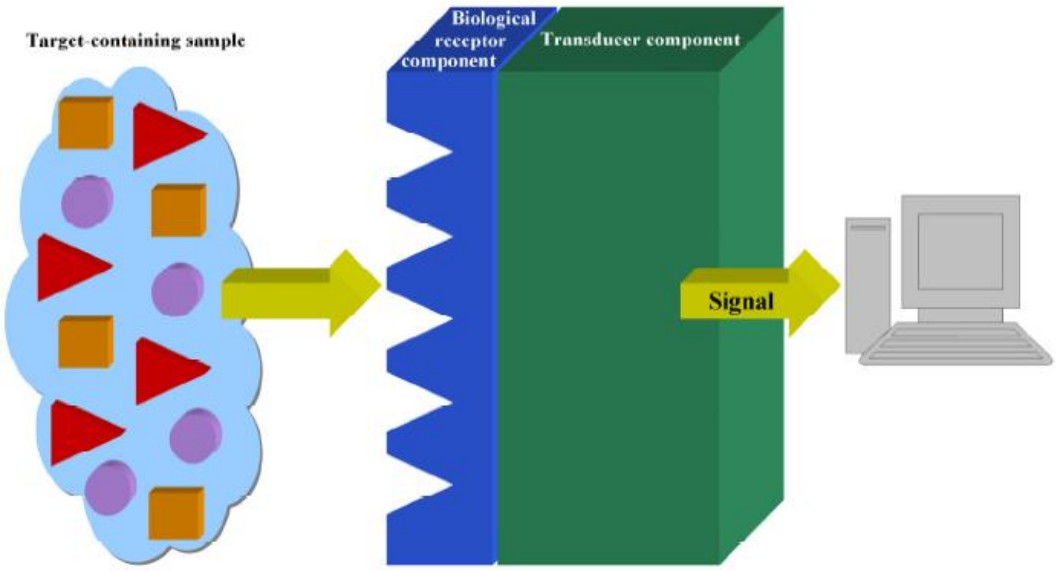


**Figure 1.1:** Schematic representation of a biosensor [10].

### 1.1.1 Receptors, transducers and bonding

The three most commonly used receptor molecules are enzymes, antibodies and DNA. Enzymes detect a target molecule and catalyze it into a reaction product which gives a measurable signal. Antibodies strongly bind to a very specific molecule or antigen, and make it a measurable antibody-protein complex. The sensitivity of the antibody sensor strongly depends on the affinity the antibody has for the target molecule. Therefore this type of biosensor is commonly referred to as an affinity-based biosensor. Since DNA consists of two complementary strands, to detect a specific sequence of DNA, the target DNA used should be ssDNA. A complementary ssDNA strand is used as receptor for the target ssDNA.

Another important aspect of a biosensor is the way it binds the receptor to the biosensor. In most biosensors, the binding of target molecule and receptor and the transduction of the signal take place in a liquid-solid interface. In order to have a sensitive and durable biosensor, the binding of the receptor molecules should therefore be as strong as possible, but should not change the biological activity of the receptor.

Binding techniques are either covalent or non-covalent. Non-covalent bonding is done by physical adsorption or by SAMs. It is the simplest way to bind the receptor to the

transducer layer, but it has some disadvantages. Physical adsorption creates a rather weak bond, yielding a non-durable sensor. In addition, sensitivity can be affected by physical adsorption. The control of orientation of the receptor molecules or proteins is almost nonexistent. If molecules and proteins are oriented at random, active regions can be concealed, and the receptor is unable to bind the target molecule.

Covalent binding of the receptor is usually preferred, but developing a working protocol can be difficult. The transducer layer can be chemically functionalized with -$HS$, -$COOH$ or -$NH_2$ groups. Biomolecules also contain these three chemical groups. Different chemical binding paths can thus be followed. A -HS group can bind with another -$HS$ group, yielding a disulfide bridge: $C$-$S$-$S$-$C$. A -$COOH$ group can bind with a -$NH_2$ group, forming a peptide bond. DNA can be modified with either of these end groups, leading to a variety of means to bind DNA to a transducer surface.

Choosing a material as a substrate depends heavily on the signal transfer used. When using a visual signal like fluorescence, a material with low backscattering is ideal. If surface plasmon resonance is used, gold is the best transducer. If an electrical signal is desired, materials with good conductivity, e.g., metals, are necessary. The use of semiconductors like silicon, germanium or gallium, however, is commoner. More recently diamond, a carbon material, has been giving very good results as a transducer in biosensors [11, 12, 4]. Nanocrystaline diamond (NCD) has good electronic properties [13] and can be doped to either a n-type of p-type conductor. It is durable because of its hardness, and it is biocompatible. This means diamond can be implanted in vivo without being attacked by the human immune system. A disadvantage of diamond, however, is the cost. NCD is grown with CVD, an expensive and slow process.

### 1.1.2 A DNA biosensor

In current medicine, biosensors are frequently used to detect DNA. The sensors most frequently used are DNA microarrays. These sensors are capable of measuring a very large number of DNA sequences at once by using multiplex technology [14]. DNA microarrays are very sensitive and have SNP sensitivity, but a fluorescent label is needed to detect the hybridization of two complimentary ssDNA strands. Because there are no cheap point-of-care DNA arrays, a cheap point-of-care DNA sensor with a simple electronic readout is still needed. Such a DNA biosensor can have SNP sensitivity and could be a great diagnostic tool for fast detection of genetic deviations and testing the sensitivity of patients to certain pathogens, chemicals and drugs. The first steps in developing this biosensor have already been taken with diamond as a transducer, by Yang and Auciello, who developed a method of covalently binding DNA to an NCD surface [15]. This protocol was further optimized and simplified by Christiaens et al. [5]. Their method of binding ssDNA to NCD was used to develop a real-time, label-free DNA sensor [4].

## 1.2 Carbon materials as transducers

Carbon is abundant in the universe. It is the backbone for life itself, and now scientists are experimenting with carbon to use it for making chips, the backbone of machines. Carbon can form up to four bonds, and because it can make double and triple bonds, it can create allotrope materials, e.g., graphite, diamond, CNT and fullerenes. The goal of this thesis is to use graphite and CNW as a transducer for biosensors. The first challenges are to bind a biological molecule to the material and to make an electrical contact.

### 1.2.1 Morphology

If a carbon atom forms four single bonds with other carbon atoms, a tetrahedral structure is formed. This material is diamond. If the carbon forms two single bonds and one double bond, it is graphite. The bonds are located in a single plane, called graphene, and form a structure that resembles chicken wire. Ordinary graphite, like in pencils, is structured in layers of graphene sheets. The layers are held together by the van der Waals force, a non-covalent bond.

It was long thought that a single layer of graphite could not exist, due to thermal vibrations in the crystal lattice which would tear it apart. This was proven true by R.E. Peierls and L.D. Landau [16, 17, 18]. However, after the discovery of CNT in 1991 [19], a new interest in exotic carbon materials led to the eventual discovery of graphene [20, 21]. In Figure 1.2, various allotrope materials of carbon are shown. The CNF and the graphene like CNW used in this thesis have the structure of graphite: they consist of stacked graphene layers.

With the CNFs, the use of "nano" in the name is debatable, since most CNFs do not have a dimension close to the nanometer scale, but rather to the micrometer scale. But the use of the name is justified because in future experiments considerably smaller flakes will be used. The CNWs also have a dimension of a few micrometers. But the thickness of these materials is four to six graphene layers, seen in Figure 1.4, thus the "nano" name is justified. Figure 1.3 displays CNWs.

### 1.2.2 Synthesis techniques

In order to make carbon materials, two things are almost always needed: a carbon source and energy. Acetylene ($C_2H_2$) or methane ($CH_4$) are frequently used as a carbon source. Heat energy [24], mechanical energy [20] or optical energy [23] can be used to break the carbon bonds from the source, and construct the needed carbon material. The CNWs are produced by Micro Wave Plasma Enhanced Chemical Vapor Deposition (MW PECVD) [23].

In MW PECVD an argon plasma is created under vacuum conditions, with a radio frequency (RF) plasma source. Methane and hydrogen are injected, and by means of

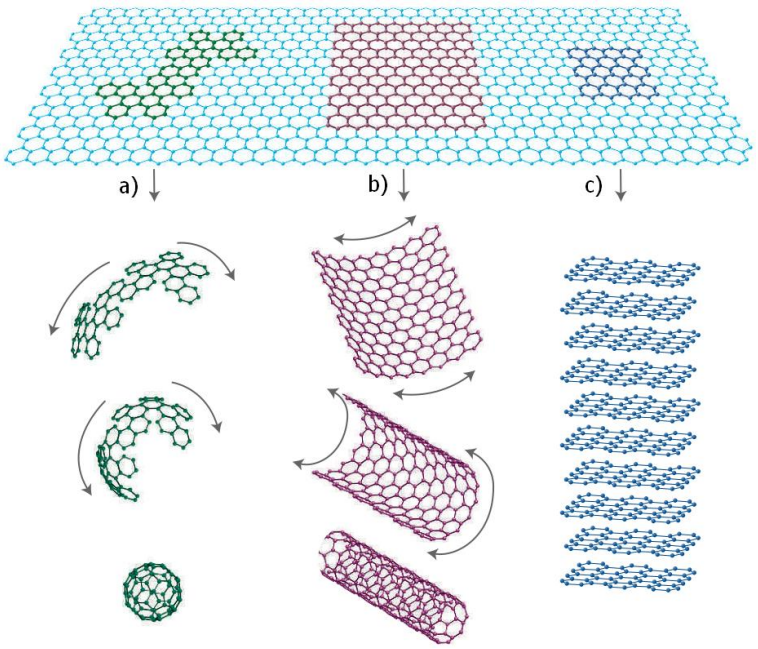


**Figure 1.2:** A graphene layer is the building block for a number of allotrope materials of carbon [22]. A fullerene is the spherical form (a), a CNT is the cylindrical form (b) and graphite is the stacked form (c).

microwaves, created by a magnetron head, the methane is split up into $CH$ radicals. These radicals attach to the substrate, and will form CNT, CNW, graphene or amorphous graphite, depending on the growth conditions. A scheme of this set-up is shown in Figure 1.5.

Graphene and CNF can be produced by mechanical or chemical exfoliation [26], or by the previously discussed CVD methods [27]. Graphene was observed for the first time by producing it with a mechanical exfoliation technique. This technique, developed by A.V. Geim [20] and K.S. Novoselov, uses sticky tape to peel off graphite and graphene flakes. A layer of HOPG, graphite which is stress annealed at 3300 K, is used as carbon source. First the graphite is sandwiched between folded tape, and the tape is slowly peeled apart. Each time this action is repeated, the flakes become smaller. Then, the tape is pressed to a substrate, and slowly pulled away. In order to detect the almost transparent flakes, a $Si/SiO_2$ substrate is used. This allows for the graphene or few-layer graphene (FLG) to be visible under an optical microscope, provided that the $SiO_2$ layer is either 90 nm or 280 nm thick [28] as in Figure 1.6. Another frequently used method to produce graphene is pressing a HOPG sample to a substrate, and rubbing the sample against the substrate, leaving graphene and FLG on the substrate.

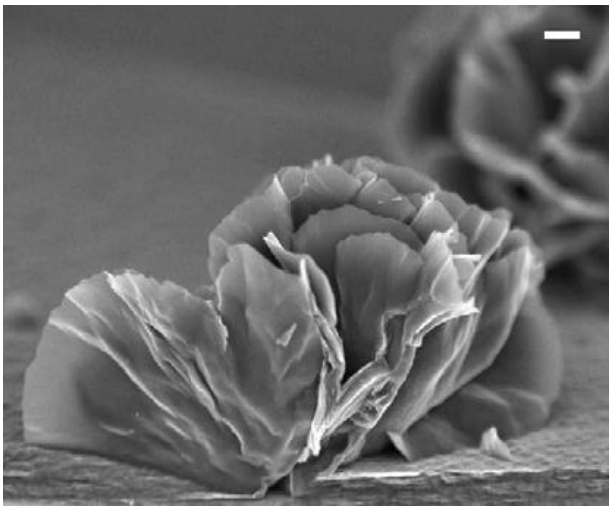

**Figure 1.3:** Cross-sectional SEM image of CNWs [23]. Because of the very large surface to volume ratio, CNWs makes an ideal transducer material to biofunctionalize with DNA. The scale bar corresponds to 1 $\mu$m.

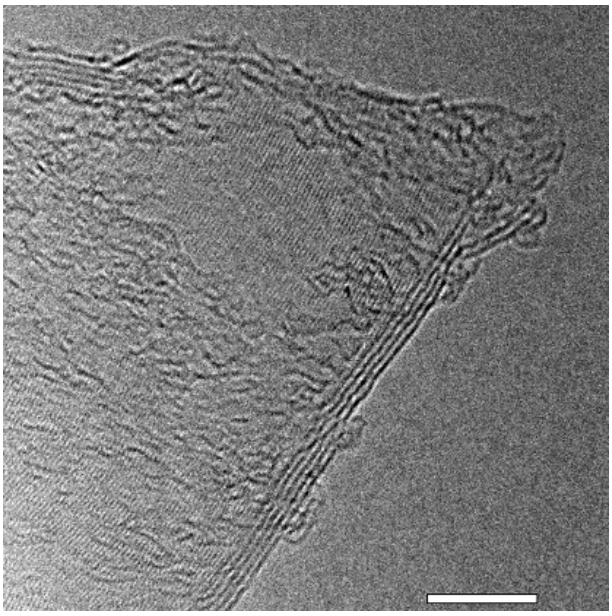

**Figure 1.4:** A TEM image of the planar shape of a CNW sheet clearly shows the thickness is between 4 to 6 graphene layers. The scale bar corresponds to 5 nm.

However, the mechanical exfoliation of graphite with sticky tape cannot be applied to

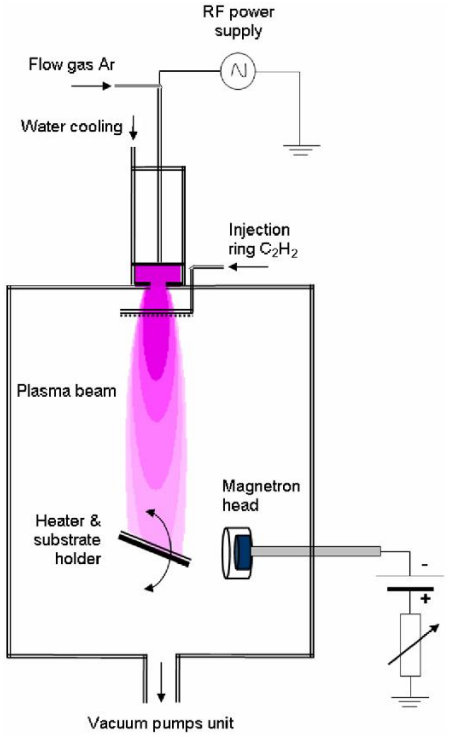


**Figure 1.5:** Scheme of a MWPECVD set-up [25].

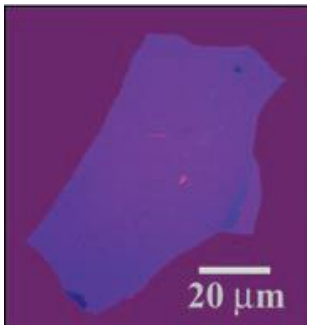


**Figure 1.6:** FLG with a thickness of 3 nm on a $Si/SiO_2$ substrate [20].

mass produced graphene, FLG and CNF. Different methods are under development. One of the most promising methods is to produce graphene by chemicaly reducing graphite oxide [29, 30].

### 1.2.3 Physical properties

The only difference between FLG and CNW are their protocols of production, which yield horizontal or vertical planes of graphite. Their physical properties are identical, although nanographite domains have been found in CNWs [31]. However, in working with nano materials, there always is a size limit beyond which the laws of classical physics stop working, and quantum rules begin to apply. In graphite, this boundary is approximately 10 graphene layers. A graphite structure with more than 10 layers of graphene will exhibit bulk graphite properties. When working with graphite consisting of fewer than 10 layers, e.g., graphene, FLG, and sometimes CNF and CNW, different rules apply. Ergo, different properties manifest.

Although the electrical properties of graphite are acceptable, there is nothing remarkable about them. Its Hall coefficient is estimated at 0.80, which indicates a deficit in electrons, and the presence of more positive holes [32]. The number of free electrons is approximately $6.10^{-6}$ per $cm^2$, the resistance ranges around $10^{-6}$ $\frac{\Omega}{cm^2}$. And graphite exhibits metallic behavior.

For graphene, the electrical properties become more exotic. For example, it is not a conductor like graphite, but rather, a gapless semiconductor. The number of charge carriers can be as high as $10^{13}$ per $cm^2$; the mobility, $\mu$, can reach 15000 $cm^2$ $V^{-1}$ $s^{-1}$ under ambient conditions [20, 33, 34]. However, mobilities of 200000 $cm^2$ $V^{-1}$ $s^{-1}$ have been reported [35], far exceeding the mobility of diamond, which is in the range of 2000 $cm^2$ $V^{-1}$ $s^{-1}$ for holes and 2200 $cm^2$ $V^{-1}$ $s^{-1}$ for electrons [36]. This is an indication of ballistic transport, present in graphene, with mean free electron paths of 0.3 $\mu$m at 300K [22]. In ballistic transport, the electrons in graphene are described with the Dirac equation, rather than the usual Schrödinger equation. So the electrons in graphene behave like quasi particles, namely massless Dirac fermions [37]. These electrons are thus moving at light speed $v_F \approx 10^6 \frac{m}{s}$.

Another curious effect which contributes to the extremely high conductivity of graphene is tunneling. In a conventional semiconductor, the chance for an electron to tunnel through a barrier is negligible. For graphene, however, the transmission coefficient is one. This implies that the electrons always tunnel through barriers, as in Figure 1.7.

To distinguish between graphite and graphene, Raman spectroscopy is a useful measurement. A Raman spectrum of carbon mainly consists of a D-,G- and 2D-band at, respectively, 1360, 1560 and 2700 $cm^{-1}$.The G-band is due to bond stretching of $sp^2$ atoms in both rings and chains. The D-band comes from the breathing modes of $sp^2$ atoms in rings and is a measurement of structural defects and impurities. The quality of a graphite sample can be determined from the R-value, the ratio of the D-band to the G-band. The R-value for HOPG should thus be zero. The difference between the spectrum of graphene and of graphite is clearly seen in the 2D-band, which splits up in graphite. A Raman spectrum of graphene and graphite is seen in Figure 1.8.

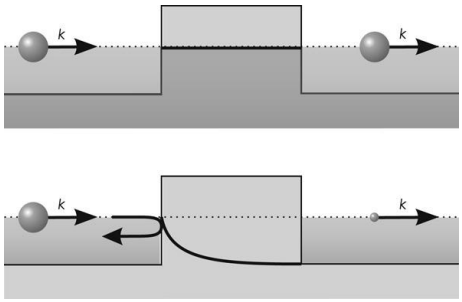


**Figure 1.7:** Top panel: tunneling in graphene. Lower panel: tunneling in a conventional semiconductor. Adopted from [38].

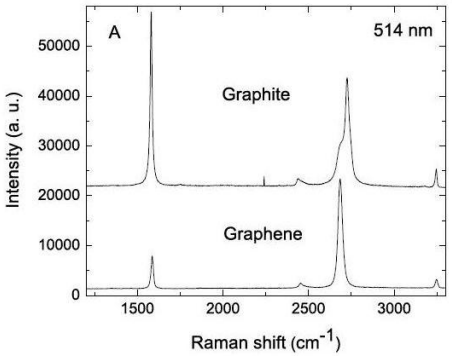


**Figure 1.8:** Raman spectrum of graphite and graphene [39].

# Chapter 2

# Materials and Methods

## 2.1 Microscopy

Light microscopy was done on an axiovert 40 MAT manufactured by Zeiss. For fluorescence microscopy, two different apparatuses were used: a confocal fluorescence microscope, Zeiss LSM 510 META, and a fluorescence microscope, Nikon eclipse 80i (Figure 2.1). For the confocal microscope measurement, the 488 nm line of an Ar-ion laser was used, which exited the label. The measurement was done above 505 nm. The confocal fluorescence microscope was used to verify covalent bonding of the NH-terminated ssDNA. The hybridization and denaturation cycles were measured with the fluorescence microscope, always with a gain of four, and an exposure time of 400 ms, unless otherwise specified. The fluorescence microscope excited the label by means of a mercury lamp. The fluorescent label used throughout the experiments was Alexa-488 because it has a very good bleaching stability. The excitation wavelength is 482 nm, and the emission wavelength is 536 nm.

## 2.2 Photolithography

Photolithography was done on a MJB3 Karl Suss Mask Aligner (MA55), Figure 2.2. A positive photoresist 7790, acquired from IMEC, Leuven, was used. The photoresist was spincoated for 30 s, at a speed of 4000 rpm, and subsequently baked at 120℃ for one minute. The resist was exposed to UV light from the mask aligner for 7.5 s. After this, OPD 5262, from Rohm and Haas, dissolved the exposed resist and etched the aluminum away. To etch the gold, a homemade $KI/I_2$ stock solution, with a mixing ratio of $KI : I_2 : H_2O = 4g : 1g : 40ml$ was used. This gives a room temperature etch rate of 1 $\frac{\mu m}{min}$ gold. This stock solution was diluted by half before use.

**Figure 2.1:** The Nikon eclipse 80i fluorescence microscope.

**Figure 2.2:** The MJBR Karl Suss Mask Aligner, with the mask on the lower left.

## 2.3 Hall setup

The Hall setup, Figure 2.3, uses the van der Pauw technique to combine a resistivity measurement and a Hall measurement. This way, not only sheet density $n_s$ and the resistivity, but also the mobility, $\mu$, can be obtained. This method was first proposed by L.J. van der Pauw in 1958 [40].

The basic principle behind the Hall effect is the Lorentz force, described by the vector equation $\vec{F} = -q\vec{v} \times \vec{B}$. If an electron travels through a magnetic field $\vec{B}$, it feels a force perpendicular to its direction of travel. If a current is applied to a bulk conductive or semi-conductive material, a buildup of holes and/or electrons will occur. A Hall voltage, $V_H$, can thus be measured perpendicular to the applied current I. The sheet density can be derived using $n_s = \frac{IB}{q|V_H|}$. By using the van der Pauw setup to determine the bulk resistivity, $\rho = R_s d$, where $R_s$ is the sheet resistance, and d is the thickness of the sample, the mobility equals $\mu = \frac{|V_H|}{R_s IB}$.

Aluminum contacts were applied to the corners of each sample, and wirebonded in a sample holder.

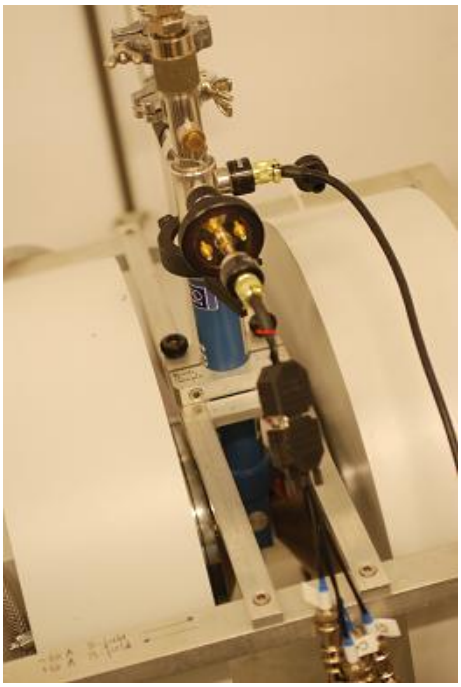

**Figure 2.3:** The Hall setup, with a Bruker B-E15v electromagnet, which allows measurements up to 1 T, and a sample holder.

## 2.4 Raman spectroscopy

Raman spectroscopy studies vibrational, rotational and other low-frequency modes in a molecule. It uses monochromatic light, usually UV or visible, which interacts with certain bonds of phonons in the molecules. The energy of the photons of the incident light is thus shifted up or down, which gives information about the phonon modes of the system, and

the molecule can be determined. Raman and infrared spectroscopy give complementary information, and the technical setup of Raman and infrared spectroscopy is very similar. Raman spectroscopy uses Stokes-Raman scattering of photons, an inelastic scattering. Infrared spectroscopy uses Rayleigh scattering, an elastic scattering.

The substrates used for Raman spectroscopy cannot be made from glass, since these are Raman active and will disturb the spectrum. Thus a silicon substrate was chosen. In order to remove any $SiO_2$ from the surface, the substrates were put into a 60 : 40 $HF$ : $H_2O$ solution for ten minutes. CNFs were brought onto the sample using the sticky tape method. To remove any sticky tape remains, the samples were annealed at 400℃ for about 30 minutes. The Raman spectroscopy was performed at Institut d'Electronique de Microélectronique de Nanotechnologie (Lille, France) by Dr. Vincent Mortet on the HOPG and CNF samples. For the CNWs, the measurement was performed by Vlaamse Instelling voor Technologisch Onderzoek (VITO), where the CNWs were made.

## 2.5 Impedance spectroscopy

Impedance spectroscopy was used to measure the impedance of the CNFs. In later experiments, when biological recognition molecules were attached to the CNF or FLG, impedance spectroscopy was required [41]. Therefore, the same setup as in impedance spectroscopy was chosen to measure resistance. The impedance spectrometer used is a HP 4194A impedance/gain-phase analyser, and is shown in Figure 2.4(a). A sample holder with a sample, ready for measurement, is depicted in Figure 2.4(b).

(a) (b)

**Figure 2.4:** (a) HP 4194A impedance spectrometer. (b) Sample holder and a glass sample with flakes and a gold electrode grid.

## 2.6 Cleaning substrates

Glass and silicon substrates were ultrasonically cleaned for 10 minutes in a soap solution. After thorough rinsing with deionized water they were put into an ultrasonic bath for 10 minutes in acetone, bought from VWR (Leuven, Belgium). In the next step, samples were put into 90℃ isopropanol, from VWR, for 10 minutes, and then blown dry with nitrogen.

## 2.7 Biofunctionalization of CNWs

In order to biofunctionalize CNWs, a linker molecule was attached to the edges. The linker molecule used was 10-undecenoic acid, obtained from Acros Organics (Geel, Belgium). It was attached to the CNW by means of photochemistry, using an UV light source, with a wavelength of 254 nm. The chemical reaction is depicted in Figure 2.5.

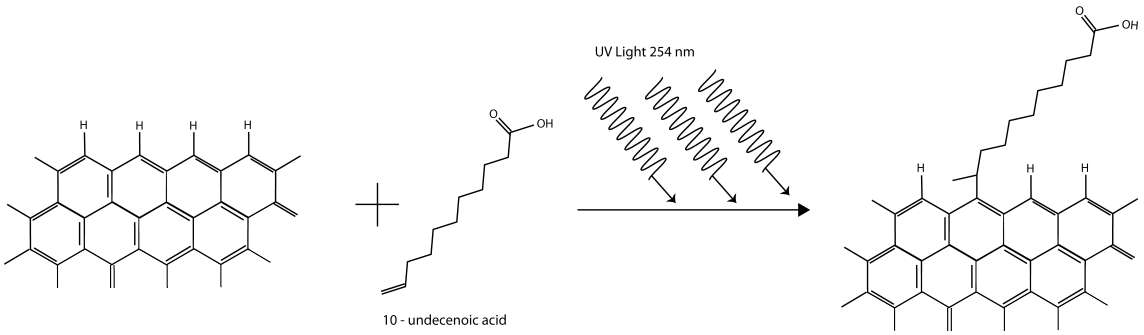


**Figure 2.5:** Attaching a linker molecule, 10-undecenoic acid, to the CNWs.

After the linker molecule was covalently bonded to the CNWs, probe DNA was attached to it. The probe DNA was chemically modified with an $NH_2$ group, in order to make an EDC-mediated bonding. Its nucleotide sequence is 5'-$NH_2$-$C_6H_{12}$-AAA-AAA-ACC-CCT-GCA-GCC-CAT-GTA-TAC-CCC-CGA-ACC-3', and was purchased from Invitrogen (Merelbeke, Belgium). Double label DNA (dlDNA) was used to directly test the covalent bonding of ssDNA to the CNW. Dl ssDNA contains the $NH-$ label to covalently attach it to the CNWs, plus the Alexa-488 label, to detect it with fluorescence microscopy. The sequence of the dlDNA is 5'-$NH_2$-$C_6H_{12}$-CCC-CTG-CA-Alexa-488-3', and was purchased from Eurogentec (Seraing, Belgium). The chemical reaction is shown in Figure 2.6.

In order to bond ssDNA covalently to the CNWs, the undecenoic acid first had to be bonded. Large samples (1 cm by 0.5 cm) and smaller ones (0.5 cm by 0.5 cm) were covered with undecenoic acid , and the samples were put under a quartz plate. Then the samples were incubated under the UV source for 20 hours. To remove the remains of the fatty acid, acetic acid ($CH_3COOH$), obtained from Sigma-Aldrich (Bornem, Belgium), was used.

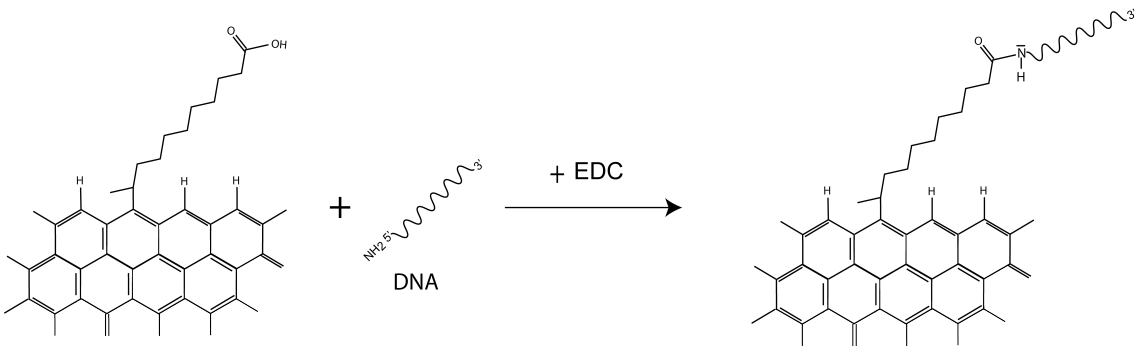


**Figure 2.6:** Covalently bonding the single stranded probe DNA to the linker molecule.

The samples were immersed into the acetic acid at 95℃ for 30 minutes. Then the samples were cleaned three times, with water at 90℃, for 1 hour. To attach the ssDNA, 30 $\mu$L 25 mM MES, obtained from Pierce (Rockford, USA), was put onto the samples. DNA was dissolved in 25 mM MES buffer, pH 6. The DNA solution was 10 $\frac{pmol}{\mu L}$. In total, 300 pmol ssDNA was added to the large samples, and 200 pmol to the small.

The solution was left to incubate at room temperature for 30 minutes. After this, EDC, obtained from Pierce (Rockford, USA), was added to cold 25 mM MES to a concentration of 50 $\frac{mg}{ml}$. In total, 15 $\mu$L of EDC solution was added for the small samples, and 20 $\mu$L for the large ones.

In the next step an extra of 15 $\mu$L MES buffer was added, and the samples were left to incubate at 4℃ for four hours. To wash away unbonded ssDNA, the samples were first put into 2x SCC : 1 % SDS over night. The SSC, saline sodium citrate, and the SDS, Sodium dodecyl sulfate, were obtained from Sigma-Aldrich (Bornem, Belgium). Then, the samples were rinsed with deionized water and immersed into a 2x SSC : 0.5 % SDS solution at 80℃ for 30 minutes. Finally, the SSC:SDS solution was replaced by 1x Phosphate buffered saline (PBS), homemade (1.29 M $NaCl$, 0.05 M $Na_2HPO_4.2H_2O$, 0.015 M $KH_2PO_4$, pH 7.4). When the CNW samples had been in the PBS solution for ten minutes, the PBS was replaced by fresh PBS, and the samples were stored at 4℃.

## 2.8 Hybridization and denaturation

Both complementary and one-base mismatch DNA, were modified at the 5' end with the fluorescent label Alexa-488. The nucleotide sequence of the complementary ssDNA strands is
5'-Alexa-488-GGT-TCG-GGG-GTA-TAC-ATG-GGC-T**G**C-AGG-GG-3'.
5'-Alexa-488-GGT-TCG-GGG-GTA-TAC-ATG-GGC-T**C**C-AGG-GG-3'

is the sequence of the one mismatch ssDNA. Both were purchased from Invitrogen (Merelbeke, Belgium).

Covalent attachment of ssDNA to the CNW was done with 300 pmol ssDNA for the large samples and 200 pmol ssDNA for the small. In order to occupy every ssDNA bonded to the CNWs with its complementary fluorescent strand, twice as much ssDNA was taken. For large samples, this meant 6 $\mu$L of ssDNA solution from a stock of 100 $\frac{pmol}{\mu L}$. For small samples, 4 $\mu$L of ssDNA solution out of the same stock was taken. The large samples were able to contain 20 $\mu$L of solution on their surfaces, while for the small samples, this amount was 15 $\mu$L. So, respectively, 14 $\mu$L and 11$\mu$L hybridization buffer, MicroHyb hybridization buffer from Invitrogen (Merelbek, Belgium), was added to the ssDNA solution before putting it on the CNW samples. In Figure 2.7, a scheme of the hybridization is depicted.

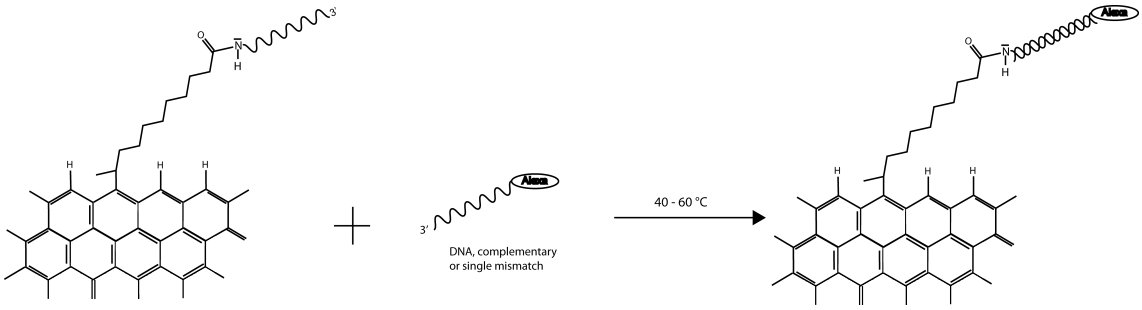


**Figure 2.7:** Scheme of hybridization of an ssDNA strand to the biofuncionalized CNWs.

The samples were put onto a polydimethylsiloxane (PDMS) surface. Because PDMS is hydrophobic, the drop of solution on the CNW was less likely to roll off the samples. In order to prevent dehydration of the CNW samples, they were placed into a saturated environment. This was achieved by adding small water droplets to the PDMS surface and sealing it from the outside environment. Next, samples were incubated in an oven at temperatures of 30, 40, 50, 60 or 70℃, for two hours.

The hybridization was then complete. But physically adsorbed DNA strands had to be removed so that only the bonded complementary or one mismatch strands remained on the surface. The CNW samples were put into a 2x SSC : 0.5 % SDS solution for half an hour. After a thorough rinsing with deionized water, the samples were put into a 0.2x SSC solution in the oven, at a temperature equal to the hybridization temperature minus 5℃, for 30 minutes. DNA dissolves extremely well in a low salt solution like 0.2x SSC, and the temperature helps by adding thermal energy to the dissolved DNA strand, which speeds the process up.

Denaturation of the CNW substrates was done with an 0.1 M $NaOH$ solution, from UCB (Brussels, Belgium), for 30 minutes, in a 50℃ oven.

# Chapter 3

# Results and Discussion

The research was divided in two main parts, to address two separate problems, biofunctionalization and electrical contact, that had to be tackled to successfully take the first steps in developing a biosensor which uses thin carbon sheets. These sheets come in two forms: vertical and horizontal. The vertically grown sheets are CNWs. The horizontal sheets are (a) the thicker CNFs, (b) the thin FLG, and (c) graphene. FLG and graphene are materials which are difficult to work with without first developing some necessary techniques to ensure electrical contact, controlled production, and accurate measurements. In this study, materials like CNWs and CNFs were used to master these techniques. However, making electrical contacts on CNWs to produce an electrical measurement platform raises some problems. For example, the CNW samples are brittle, and making contact with a single sheet is practically impossible, since they form networks. The carbon flakes, or potentially, the CNFs, lie horizontally on a surface. They can be easily produced. Also, the samples proved to be very robust, and capable of withstanding some mishandling.

## 3.1 Fluorescence measurements

### 3.1.1 Covalent bonding of ssDNA to CNWs

To directly test the covalent bonding of ssDNA to the CNWs, an Alexa-488 labeled probe DNA (dlDNA) was used. Due to growing conditions, the CNW do not have a completely uniform surface. Most of the surface was covered with CNWs, but some "naked" parts were covered with amorphous graphite layers. In Figure 3.1 the fluorescence intensity of the CNWs, which were biologically modified with the double label probe DNA, is shown.

In Figure 3.1, it is clearly seen that the signal intensity of the surface, covered with CNWs, Figure 3.2(b), is higher than the intensity of the surface covered with amorphous graphite,

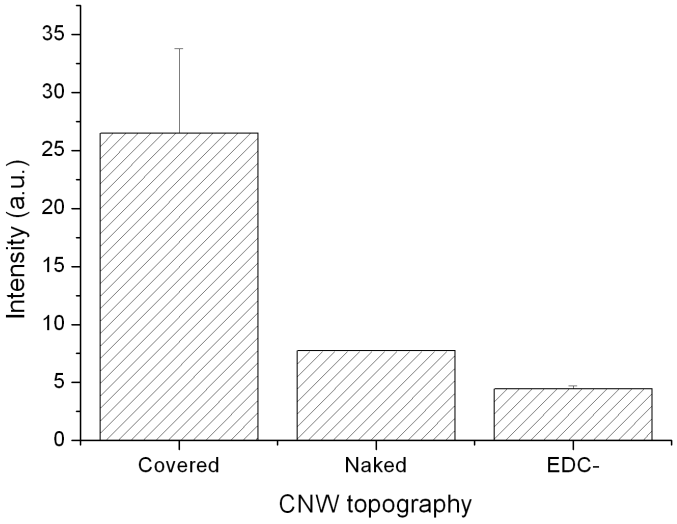


**Figure 3.1:** Histogram of an average fluorescence intensity, taken from 2 CNW samples, modified with double label probe DNA. The EDC- is a control sample.

Figure 3.2(c). The difference in intensity is approximaly 8.7 a.u., or a decrease in fluorescence by 48%. This difference in bonding capacity is attributed to the fact that CNWs have more hybrogen terminated bonds than amorphous graphite. Since the photochemical method of covalently bonding the DNA to the carbon surface doesn't have enough energy to break a $C-C$ bond, the bonding happens at the edge of the carbon plane. This means that when graphene is functionalized with this method, only the contour, and occasionally defects in the crystal latice, are modified. Since CNWs, as seen in Figure 1.3, would have a greater number of hydrogen terminated bonds, they are capable of binding more ssDNA to their surface then regular amorphous graphite, because of the large surface to volume ratio. The negative control sample, Figure 3.2(a), is a sample where, instead of the EDC solution, regular 25 mM MES was added. Since the bonding of DNA is mediated by EDC, the fluorescence intensity was attributed to physical adsorbtion. When comparing the fluorescence intensity of the EDC- sample with the positive sample, the difference clearly proves covalent bonding.

A confocal fluorescence microscope can clearly show the covalent bonding of ssDNA to the CNWs. In Figure 3.3, a photograph of a CNW sample, which was hybridized with complementary ssDNA is shown. With confocal fluorescence microscopy, a small section of the surface can be bleached. This means that the laser will scan repeatedly over the same spot, with high intensity. This effectively burns the Alexa-488 label, attached to the ssDNA, and the bleached spot loses fluorescence.

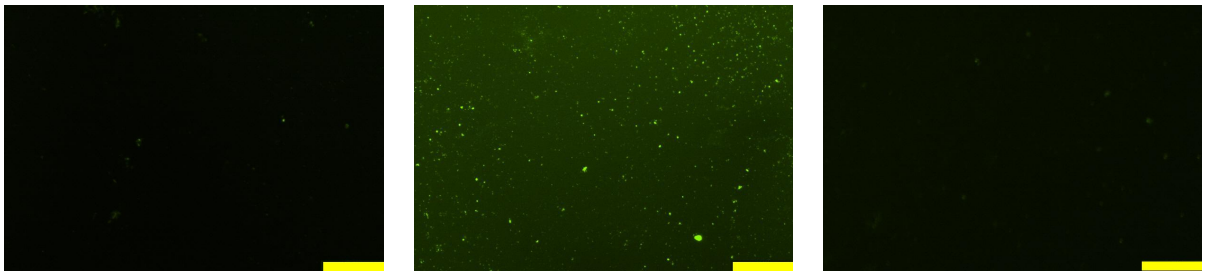

(a) (b) (c)

**Figure 3.2:** (a) Fluorescence microscopy photo of the EDC- dlDNA CNW sample. (b) Fluorescence microscopy photo of the EDC+ covered dlDNA CNW sample. (c) Fluorescence microscopy photo of the EDC+ naked dlDNA CNW sample. The line on the lower right of the three figures corresponds to 100$\mu$m.

In order to try to improve the covalent attachment of the undecenoic acid to a CNW, certain samples were boiled in deionized water for two hours, and others were put into sulfuric acid ($H_2SO_4$) at 95℃, also for two hours. After these treatments, probe DNA was attached the same way as in other samples, and hybridization experiments were done. The result of those hybridizations are seen in Figure 3.4.

It is clear that modifying the surface of the CNWs by means of boiling in water or by putting it into sulfuric acid does not improve the fluorescence intensity after hybridization. In fact, intensities from the $H_2SO_4$ and boiled samples are, respectively, 11.2 and 11.8 a.u. This is approximately 41% less than the untreated sample.

### 3.1.2 Optimizing hybridization conditions

Hybridization of two DNA strands can be done at temperatures ranging from 20℃ to 80℃. Going below 20℃ will make it difficult for two complementary strands to bond. The thermal velocity of the DNA strands is too low to allow two strands combine to within a reasonable time frame, i.e., two hours. The thermal energy of the strands, when the temperature rises above 90℃, is too high to keep them together. The denaturation temperature of two strands is 95℃.

In order to hybridize within these two extreme temperatures, five temperatures (30, 40, 50, 60 and 70℃) were chosen to find the optimum hybridization temperature. In Figure 3.5, an average over three consecutive hybridizations is given.

The hybridization was done with complementary ssDNA. The data shows that hybridiza-

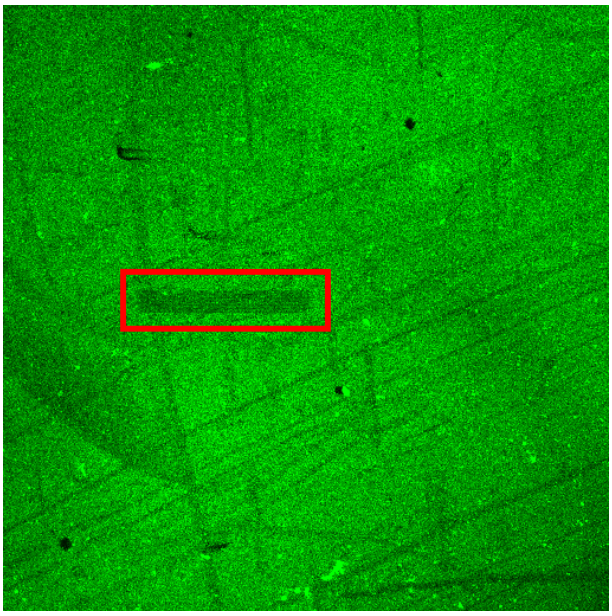

**Figure 3.3:** Image taken with the confocal fluorescence microscope. Hybridization was done with complementary DNA, and at 60℃. The red rectangle indicates a small surface that was bleached. The image is 900$\mu$m by 900$\mu$m.

tion at 40℃ and 50℃ yields the best results. Hybridization at 30℃ yields a system with low thermal energy. If a sufficient fluorescence intensity at 30℃ is desired, a longer hybridization time will be required. The other extreme, 70℃, is too high to let all the ssDNA in the solution bind to a complementary partner. Although the fluorescence intensity of the samples hybridized at 30℃ is greater than the intensity of the 60℃ samples, the difference in 1MM and COM for the 30℃ samples is not significant, Figure 3.6. Only strands that are positioned perfectly on the CNWs, without disturbance of external factors, will bind an ssDNA molecule from the solution.

The smallest deviation in DNA sequence possible is one base pair. These faults in the genome of a patient are called single nucleotide polymorphisms (SNPs). To detect SNPs, a sensor should be able to detect the difference between a completely complementary strand, and a strand with just one base pair that is different from the complementary strand: one mismatch ssDNA. To test the sensitivity of the sensor setup, hybridization between one mismatch (1MM) and complementary (COM) DNA was compared. The varying fluorescence intensity between 1MM and COM ssDNA was caused by affinity in function of temperature. Measurements were thus done with a temperature gradient with temperatures of 40, 50 and 60℃. The results are shown in Figure 3.7.

Figure 3.7 clearly shows that the difference in binding strength between complementary

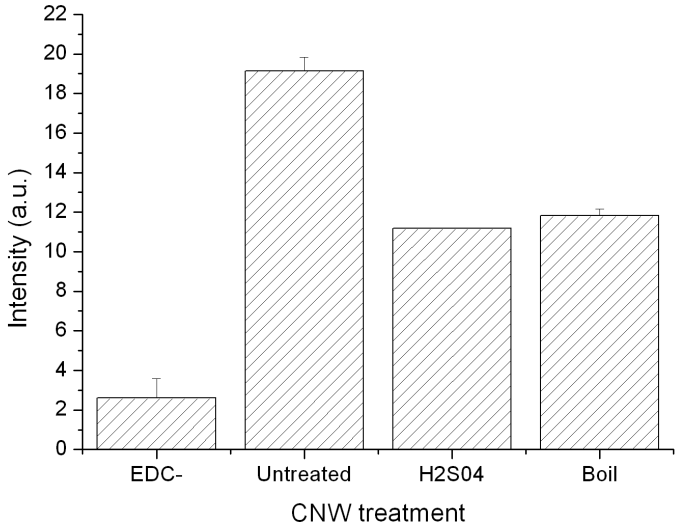


**Figure 3.4:** Histogram of average fluorescence intensity, taken over two hybridizations, of surface modified CNW samples. The EDC- is a control sample.

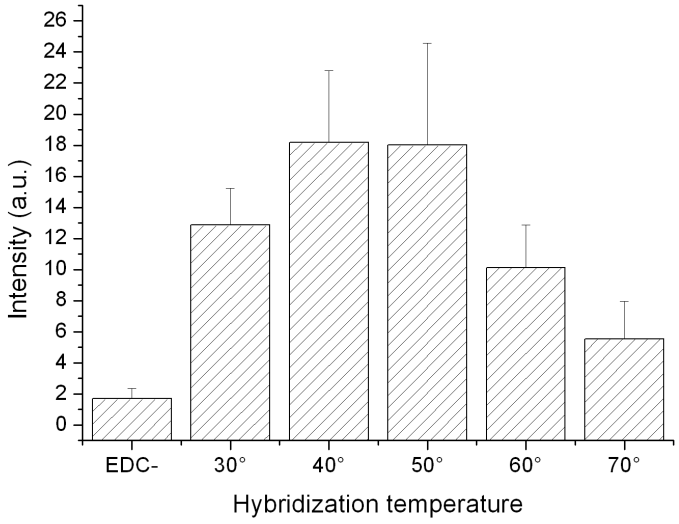


**Figure 3.5:** Histogram of an average fluorescence intensity, taken over 3 hybridizations. The EDC- is a control sample.

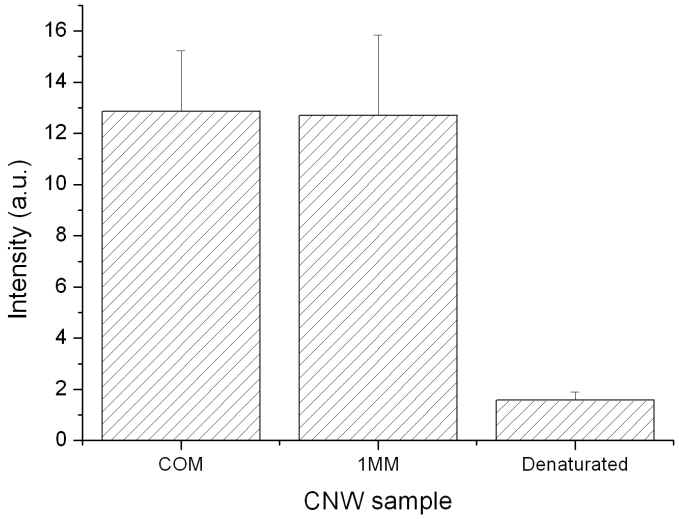


**Figure 3.6:** Difference in intensity of 1MM and COM hybridization at 30°C. The data show no significant change in fluorescence intensity.

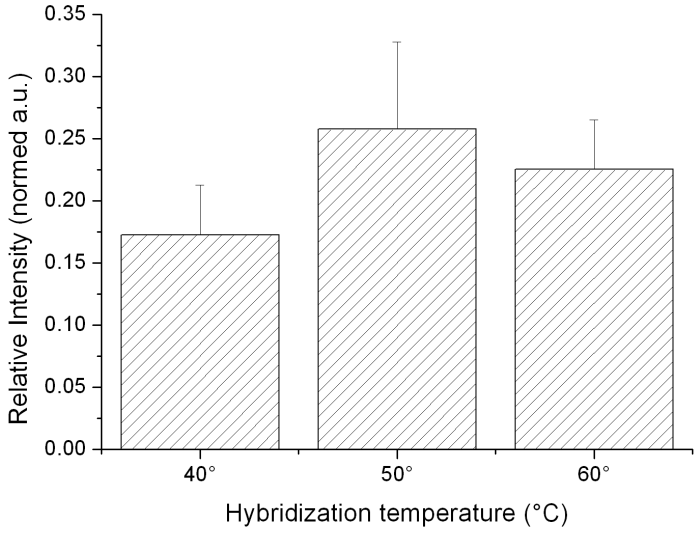


**Figure 3.7:** Histogram of relative average fluorescence intensity, taken over five hybridizations, to show the difference between hybridization with COM DNA and 1MM DNA.

strands and one mismatch strands is proportional to the temperature. When the system has a higher thermal energy, there is more energy available to break bonds between two DNA strands. The bonding strength between two complementary strands is greater than the bonding strength between one mismatch strands. However, this does not explain why hybridization done at 50℃ leads to the highest selectivity, and why hybridization at 60℃ leads to a diminished capability to distinguish 1MM DNA from COM DNA. This is attributed to the fact that the fluorescence intensity of the hybridization at 60℃ is far less then the intensity at 40 or 50℃. Hybridization at 60℃ is too ineffective to sufficiently bind ssDNA molecules, whether they are complementary or one mismatch. Since only two samples per temperature were used, one of which was hybridized with mismatch DNA, and the other with complementary DNA, the sample related difference had to be ruled out. This is done by switching the complementary and one mismatch samples every other hybridization cycle. In Figure 3.8(a), 3.8(b) and 3.8(c) respectively an EDC- control sample, a sample hybridized at 50℃ with COM DNA and a CNW sample hybridized at 50℃ with 1MM DNA are shown.

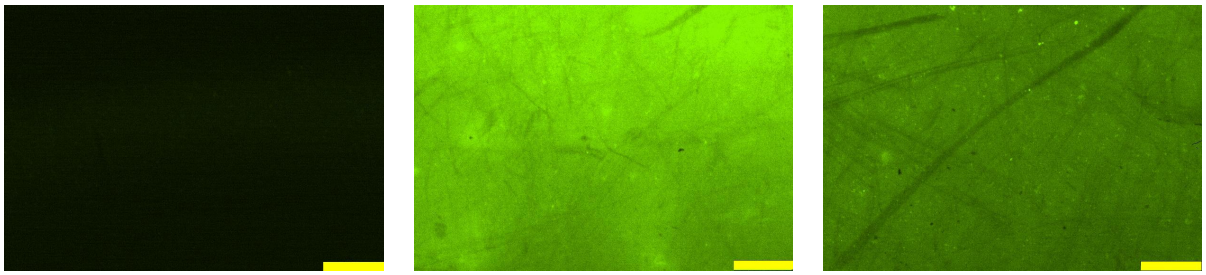

(a) (b) (c)

**Figure 3.8:** (a) Fluorescence microscopy photo of the EDC- CNW sample, at a gain of x16. (b) Fluorescence microscopy photo of a sample which is hybridized with complementary ssDNA at 50℃, with a gain of x16. (c) Fluorescence microscopy photo of a sample which is hybridized with one mismatch ssDNA at 50℃, with a gain of x16. The line at the lower right of the three figures corresponds to 100$\mu$m.

### 3.1.3 Investigating reusability

If a cheap point-of-care sensor is developed, reusability is an important aspect to keep costs low. To investigate reusability, consecutive hybridization cycles were performed. One hybridization cycle consists of a hybridization, followed by a denaturation of the samples by means of 0.1 M $NaOH$. The hybridization, at 40, 50 or 60℃, was repeated for nine cycles plus one hybridization. After the first five cycles, the complementary and one

mismatch hybridized samples were switched every cycle. In Figure 3.9, the intensity over all hybridization cycles is shown.

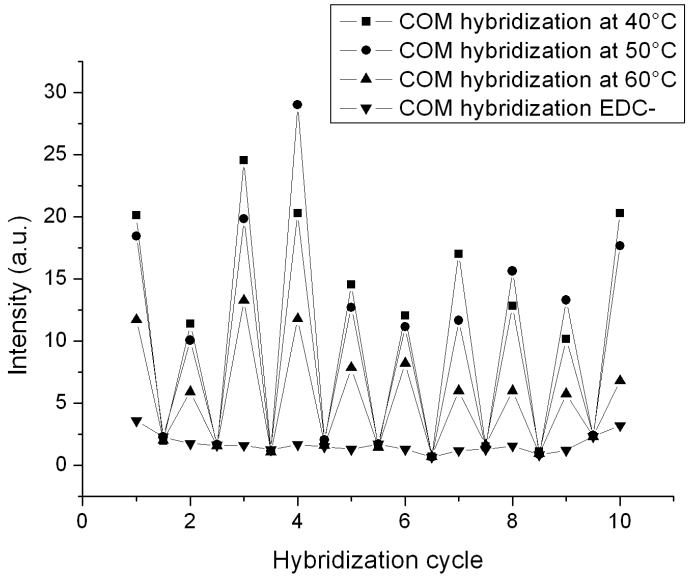


**Figure 3.9:** Graph of the hybridization cycles with hybridization temperatures 40, 50 and 60℃. The negative controle sample, EDC-, was hybridized at 40℃with COM DNA.

In Figure 3.9, it is clearly seen that a sensor based upon CNW, or related materials, can be reused for at least ten tests. The second hybridization for all samples showed an intensity significantly below the average. This was due to an inconsistency in protocol, but the cause was not found. Overall, the intensity of 40℃ and 50℃ samples was good, but after the fourth hybridization cycle there was a sudden drop. This is attributed to the fact that, for the fifth hybridization, the switching of complementary samples to one mismatch was started. This indicated a lower level of previous fluorescence for those samples, due to CNW quality. Since for every temperature only two samples were used, not counting the EDC- sample, it is likely that, on average, the mismatch samples were less biofunctionalized and thus gave a lower fluorescence intensity after hybridization. Similar to Figure 3.5, the graph in Figure 3.9 again shows that hybridization at 40℃ and 50℃ leads to the best intensities. The fluorescence intensity of the sample hybridized at 60℃ is again less.

Every hybridization was followed by a denaturation. The fluorescence intensity after denaturation was significantly less. This is proof of specific hybridization and not adsorption. Lack of fluorescence intensity of the EDC- sample again proves hybridization, rather then physical adsorption.

## 3.2 Measuring physical properties

In order to measure impedance, it is necessary to make contact with the CNF. Since the carbon flakes had a size in the range of 10 $\mu$m, photolithography was necessary to make a closed electrical circuit. Raman spectroscopy was used to measure the quality of the flakes, and to see if the flakes are still bulk graphite or were behaving more like graphene or FLG.

### 3.2.1 Creating stable contact with the CNFs

An important aspect of making a stable contact with the carbon flakes is the sample preparation. Two methods were tested: carbon flakes in suspension, and flakes deposited on a glass substrate by the method developed by A.K. Geim and S.V. Novoselov.

In the first method, a HOPG layer was taken from the bulk sample by sticky tape. After this, the carbon was split by folding the tape, then pulling it apart again. After this was done ten times, a piece of sticky tape was cut off with a scalpel and put into a solution of methanol, acetone, isopropanol or SDS buffer. These four solutions, with sticky tape floating in them, were put in an ultrasonic bath. The ultrasonic bath loosened the CNFs from the sticky tape, and broke it in even smaller pieces. Then the solution was put to rest for 90 minutes, to let the flakes sink to the bottom. When the supernatant was removed from the solution, the tape remains were largely removed, increasing the flake concentration.

The methanol solution failed to remove the carbon flakes from the tape. Acetone and the SDS buffer completely dissolved the tape, polluting the sample and causing the flakes and the tape remains to stay on the glass substrate when the solution evaporated. Isopropanol, however, was an ideal solvent: It loosened the flakes from the tape without affecting the tape itself, and dried quickly. Only limited residue from the tape remained on the substrate.

To remove the remaining tape residue left by the isopropanol solvent, samples were heated at 400℃. The results are seen in Figure 3.10. Heating greatly improved the visual quality of the samples. The tape residue appeared to be completely removed, and flakes were brighter, indicating reduced sticky tape pollution. However, impedance could not be measured, either with aluminum or gold electrodes. Scanning Electron Microsopy (SEM) images revealed damage to the electrodes, preventing contact between the carbon flakes and the electrodes. SEM images are shown in Figure 3.11.

When Geim and Novoselov's method was used, the amount of tape residue was greatly diminished, and stable contact with the flakes was possible. In Figure 3.12, two samples are shown which are prepared using their method.

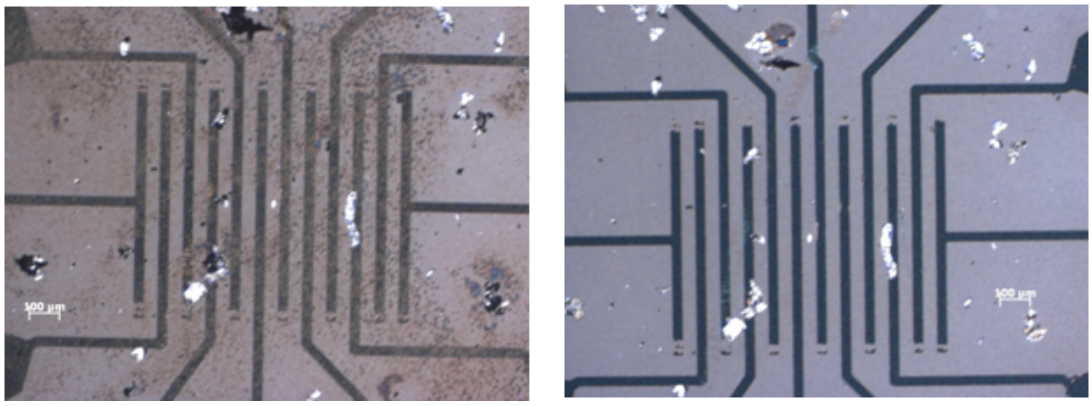

(a) (b)

**Figure 3.10:** (a) Sample before heating. (b) Sample after heating.

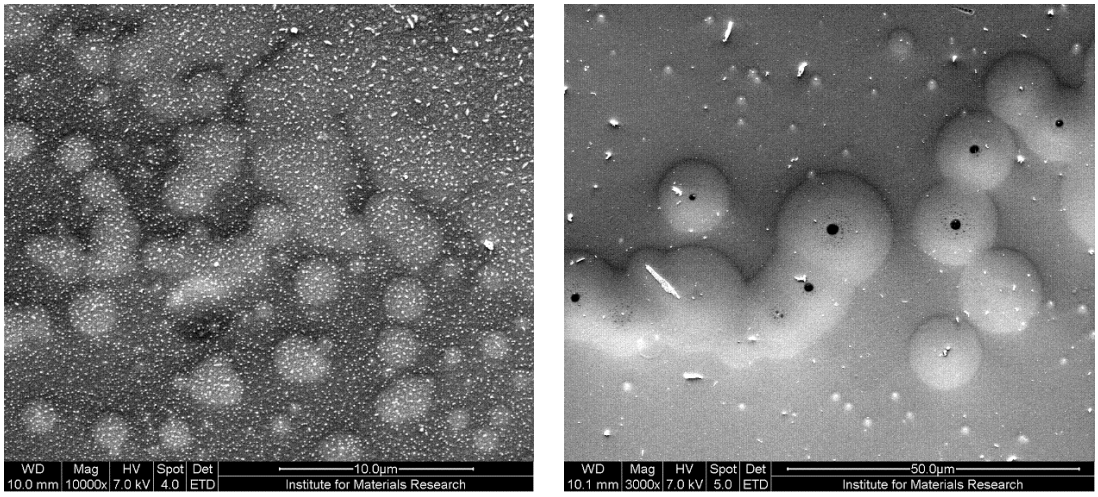


(a) (b)

**Figure 3.11:** In both (a) and (b), damage to the aluminum electrode surface is seen. Figure (b) indicates tape residue is not completely removed from the substrate after heating, but rather, has spread out and formed dome-like structures on the glass substrate. Since the formed structures are of the order of 10 $\mu$m, the same as the flakes and the interdigital electrodes, it is plausible that they disturb electrode contact with the CNFs.

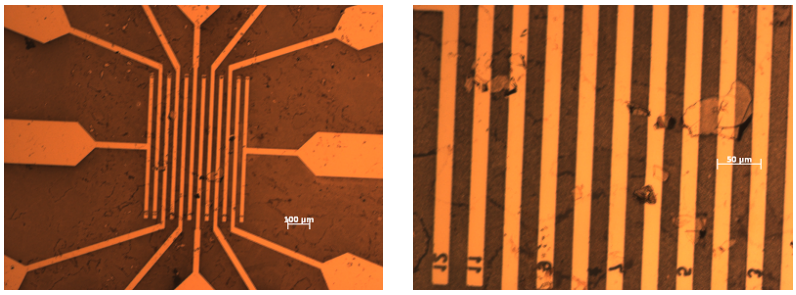

(a) (b)

**Figure 3.12:** Flakes, overlaid with an array of gold electrodes. (a) Magnification of 5x. (b) Magnification of 20x.

### 3.2.2 Impedance measurements

In order to develop a sensor with an electronic readout, impedance spectroscopy can be used to detect the hybridization between two complementary or one mismatch ssDNA strands. The hybridization of ssDNA to the surface changes both surface conduction and capacitance. These changes can be detected by impedance spectroscopy. In order to develop a fast and sensitive sensor, the resistance of the transducer should be as low as possible. Therefore impedance measurements, to determine the resistance or impedance, were done. Also, the same setup can be used in later research, when the CNFs are biofunctionalized.

In Figure 3.13, the impedance is plotted against the frequency. Both samples have an impedance of the same magnitude, and the graphs show a similar shape. The curves are approximately linear, with only a small deviation at high frequencies. This shows that the flakes are purely resistive. The deviation of the linear behavior at high frequencies can be attributed to electrode contact effects and wiring of the measurement setup. Compared to diamond, a material currently used in a similar DNA sensor setup, the resistance of the CNFs is considerably lower. At low frequency, the resistance of the CNFs is in the range of tens of $\Omega$, and diamond is in the range of k$\Omega$, [4]. In Figure 3.14 and 3.15, the measured flakes are shown.

Figure 3.14 shows that some photoresist remains. It does not interfere with the measurement, since the electrodes are on top of the carbon flakes.

In order to test the effect of the electrodes, a drop of silver paste was put on the interdigital electrodes of the gold electrode grid to shortcut the circuit. When the impedance was measured, the influence of the electrodes on the impedance was determined. The result of the measurement is shown in Figure 3.16.

Since both Figure 3.16 and Figure 3.13 show a more nonlinear behavior in high frequencies,

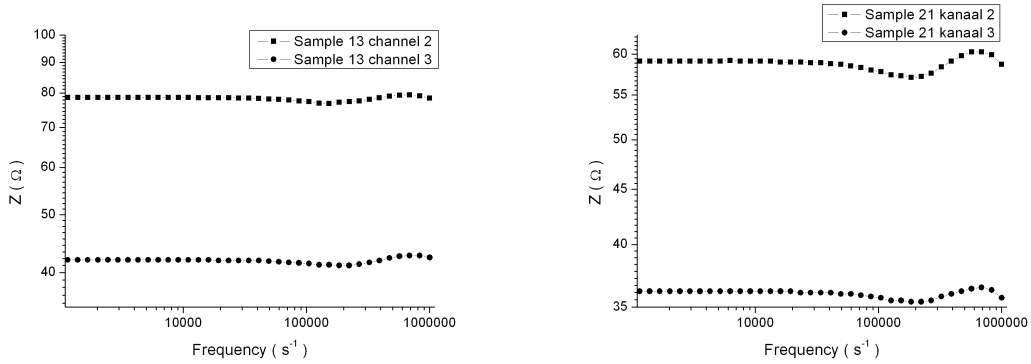


(a) (b)

**Figure 3.13:** Graphs of the impedance measurements on two samples, each of them containing two measured carbon flakes.

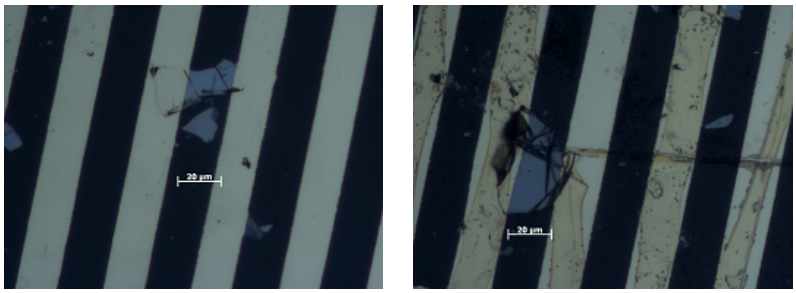

(a) (b)

**Figure 3.14:** (a) Carbon flake sample 13 measured with channel two. (b) Carbon flake sample 13 measured with channel three.

this proves that the carbon flakes have only resistive properties. Phase changes in high frequencies were thus caused by the electrode contacts, not by the carbon flakes. Since an impedance around 10 Ω and 12.5 Ω was found for the electrodes, the impedance of the flakes was affected and it could be reduced by using a four-point measurement to counter electrode effects.

### 3.2.3 Raman spectroscopy

Raman spectroscopy can indicate the thickness of the flakes (graphite, FLG or graphene) and give a ratio of quality (crystallinity) when comparing the D-band and G-band to give

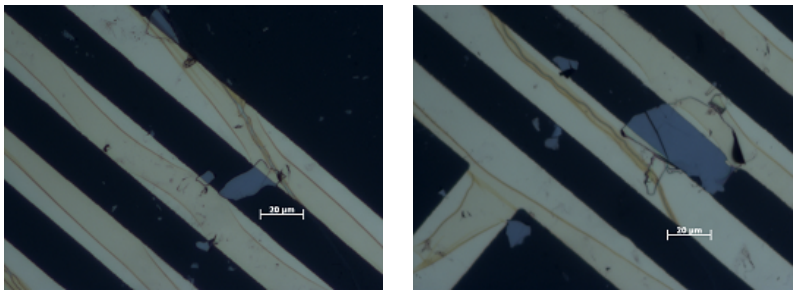


(a) (b)

**Figure 3.15:** (a) Carbon flake measured with channel two from sample 21. (b) Carbon flake measured with channel three from sample 21.

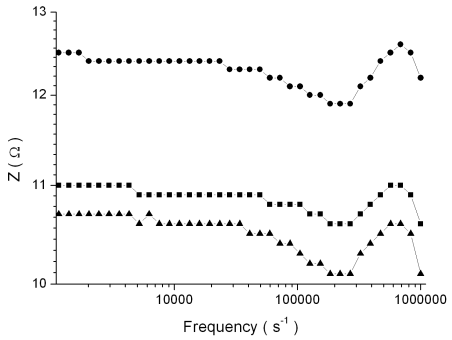


**Figure 3.16:** Impedance measurement to determine the effect of the electrodes on the impedance measurement of the carbon flakes.

an R-ratio. The flakes were prepared using the method of A.K. Geim et al. and put onto a Si substrate, since this does not give a Raman signal. In Figure 3.17, a light microscope image of the substrate is given. Two points, G1 and G2, are indicated. A Raman signal of those two points was obtained.

The Raman spectrum was taken with a UV laser as incident light, and with a laser with a wave length of 488 nm. In Figure 3.18, a spectrum taken with 488 nm light is shown. Both measured points do not have a visible D-band. The R-ratio is thus zero, meaning the flakes are of perfect quality, and have a total crystalline structure. In order to distinguish graphite from graphene or FLG, the 2D-band was examined. In Figure 3.19, this is shown for the measure point G1, both for the spectrum taken with UV and 488 nm light.
In both spectra, the 2D-band exhibits a shoulder, meaning it is graphite. In the Raman spectrum taken with UV light, the 2D-band has shifted, but it exhibits a more prominent

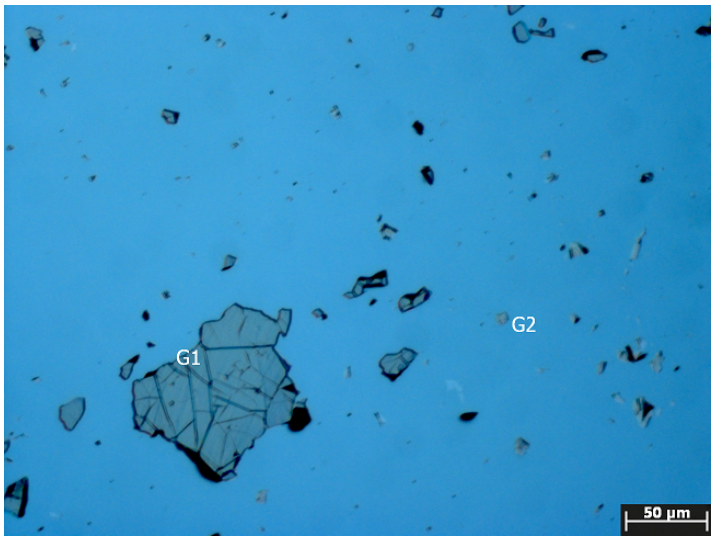


**Figure 3.17:** Image of a Si substrate with flakes, two points G1 and G2 indicate where a Raman spectrum will be determined.

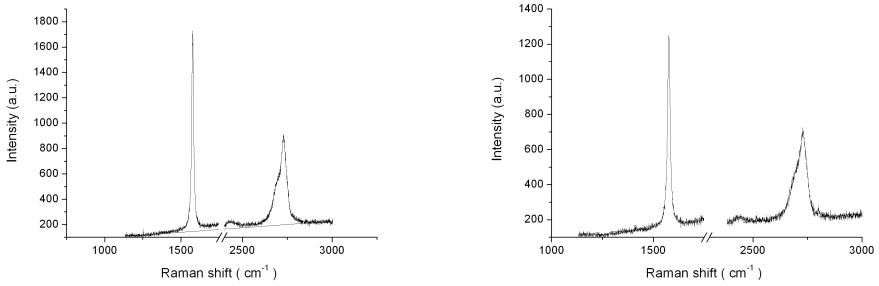


(a) (b)

**Figure 3.18:** (a) Raman spectrum of G1. (b) Raman spectrum of G2. Both taken with incident laser light with a wave length of 488 nm.

shoulder. For HOPG, the Raman spectrum was also taken with UV light, as shown in Figure 3.20. The 2D-band of the HOPG sample is similar to the one at point G1, giving further evidence that the flake is thick and clearly graphite.

In Figure 3.19, the Raman spectrum for the flake at point G1 is shown. Graph (b) of Figure 3.19 shows the spectrum for incident light of 488 nm. A small shoulder is visible but it is not as explicit as the shoulder in the 2D-band taken at the G2 point. When looking at the 2D-band of the Raman spectrum taken with UV light, the difference between the measuring

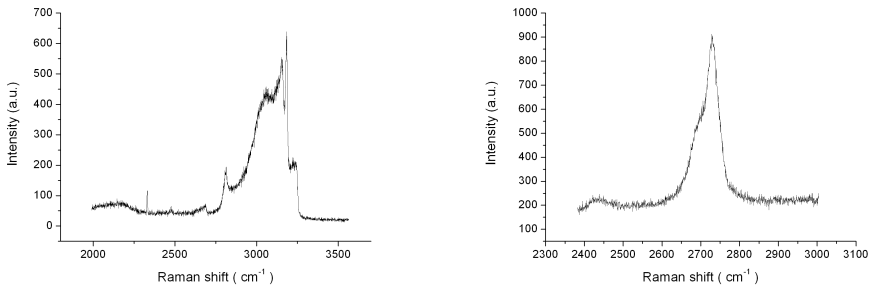


(a) (b)

**Figure 3.19:** (a) Raman spectrum of G1 taken with UV light. (b) Raman spectrum of G1 taken with 488 nm light.

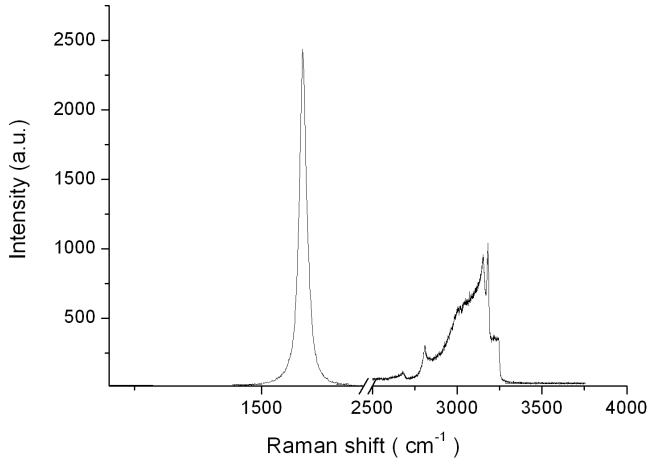


**Figure 3.20:** Raman spectrum of a HOPG sample, taken with a UV laser.

points G1 and G2 is clear. The spectrum at G2 does not show the explicit shoulder from the 2D-band seen in the spectrum at G1. This indicates that the smaller flake of point G2 is thin, and does exhibit properties leaning more to FLG and graphene. Impedance measurement of such small flakes was not attempted, since the photolithography is not precise enough to make electrical contact with such small structures.

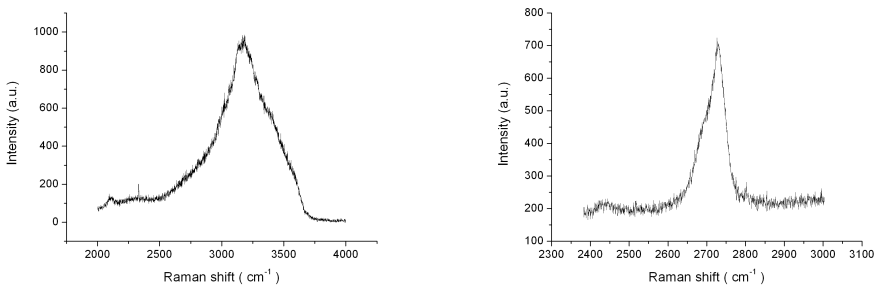


(a) (b)

**Figure 3.21:** (a) Raman spectrum of G2 taken with UV light. (b) Raman spectrum of G2 taken with 488 nm light.

### 3.2.4 Hall measurement

To test the electrical properties of the CNWs, Hall measurements and resistivity measurements were done with a van der Pauw setup. The results of both measurements are shown in Figure 3.22.

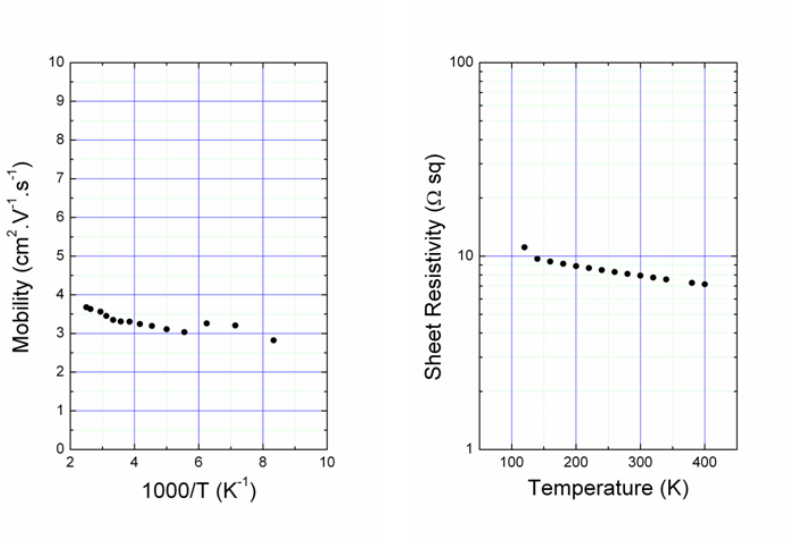


(a) (b)

**Figure 3.22:** (a) Mobility of a CNW sample. (b) Measured resistivity of a CNW sample.

The mobility of the charge carriers in CNWs, shown in Figure 3.22 (a), is very low compared to the mobility of FLG and graphene. This can be explained by the fact that the CNWs

formed networks, and different sheets were measured, reducing the mobility. Also, the network may not be uniform, in the sense that it can be disconnected at some place. The charge carriers will then move through the amorphous graphite, which diminishes mobility. The resistivity of around 10 Ω, again, higher then FLG or graphene, can also be explained by network forming and network disconnection.

The mobility curve increases with higher temperatures. This is normally only seen in semiconductors. Bulk graphite exhibits metallic conductivity, but the properties of graphene or FLG do depend on the shape of the edges, zigzag or armchair, giving respectively more metallic or semiconductive behavior. Another possible explanation of the observed effect may be the influence of the silicon substrate. Since Si is a semiconductor, the semiconductive behavior can be attributed to the Si substrate itself.

# Chapter 4

# Conclusion and Synthesis

When testing the possibility of biofunctionalizing CNWs with ssDNA, the Alexa-488 labeled probe ssDNA proves covalent attachment. The EDC- and EDC+ samples rule out any physical adsorption effects. If regular ssDNA with an $NH_2$- label to bind to the hydrogen bonds of the CNWs is used, hybridization experiments are possible. Again, EDC- and EDC+ samples show a good covalent bond between the DNA and the CNWs. When hybridization experiments are done, there is a clear difference in fluorescence intensity between the hybridized and the denaturated samples. This shows that the ssDNA is still biologically active and can bind a complementary ssDNA molecule.

In order to test the selectivity and hybridization of the bonded ssDNA, the difference in fluorescence intensity between complementary and one mismatch ssDNA was measured. Since one mismatch ssDNA only differs in one base pair, SNP sensitivity of the sensor is thus possible. The difference between the hybridization intensity of complementary and one mismatch ssDNA is statistically significant in hybridization temperatures of 40℃ 50℃ and 60℃.

The ultimate goal is to incorporate the detection of ssDNA plus the difference between complementary and one mismatch strands in a electronic platform. Therefore electrical contacting should be possible with the carbon structures. This was proven by doing an impedance measurement on a flat, horizontal CNF. At first aluminum was used, but the contact between the carbon structure and the aluminum was not sufficient for a successful electrical measurement. Therefore, gold was used as electrode material. An array of interdigital gold electrodes was deposited onto the CNFs by using photolithography. The impedance measurements were successful, and an impedance in the range of 50 Ω was found. This is far less then current transducer materials used in DNA sensor research, making it possible to develop a more sensitive sensor by using CNFs or eventually FLG or graphene.

Using a van der Pauw setup, Hall and resistivity measurements were performed on the

CNWs. The mobility of the CNWs was lower than expected, compared to similar carbon structures like FLG. But lack of homogeneity of the CVD grown CNWs may explain that. Also, the mobility shows semiconductor properties. One explanation can be that the surface edges of the CNWs are armchair-shaped, leading to the semiconductor properties. The second explanation is that, since the substrate on which the CNWs were grown is silicon, the properties of Si were measured. Further measurements on CNWs grown on a quartz substrate are thus necessary.

Since CNFs are easier to connect to electrodes then CNWs. The goal for the future is to covalently bond ssDNA not only to dangling bonds, but also to the surface of the CNFs. This way, the flat and horizontal CNFs can be hybridized completely, and electrical detection of the binding between the bonded ssDNA and the complementary or one mismatch ssDNA in solution can be achieved. Furthermore, the size of the CNFs can be reduced if e-beam lithography is used. In principle, using FLG or graphene should make the proposed sensors even faster and more sensitive.

# Bibliography


[1] Zeng YL, Huang YF, Jiang JH, Zhang XB, Tang CR, Shen GL, et al. Functionalization of multi-walled carbon nanotubes with poly(amidoamine) dendrimer for mediator-free glucose biosensor. Electrochemistry Communications. 2007;9(1):185–190.

[2] Johnson A, Staii C, Chen M, Khamis S, Johnson R, Klein M, et al. DNA-decorated carbon nanotubes for chemical sensing. Physica Status Solidi B-Basic Solid State Physics. 2006 Nov;243(13):3252–3256.

[3] Yang W, Moghaddam MJ, Taylor S, Bojarski B, Wieczorek L, Herrmann J, et al. Single-walled carbon nanotubes with DNA recognition. Chemical Physics Letters. 2007 Aug;443(4-6):169–172.

[4] Vermeeren V, Bijnens N, Wenmackers S, Daenen M, Haenen K, Williams OA, et al. Towards a real-time, label-free, diamond-based DNA sensor. Langmuir. 2007;23(26):13193–202.

[5] Christiaens P, Vermeeren V, Wenmackers S, Daenen M, Haenen K, Nesladek M, et al. EDC-mediated DNA attachment to nanocrystalline CVD diamond films. Biosensors & Bioelectronics. 2006 Aug;22(2):170–177.

[6] jr Clark LC. Monitor and controle of blood and tissue oxygen tensions. American Society for Artificial Internal Organs. 1956;2:41–48.

[7] Ly SY, Lee CH, Jung YS. Voltammetric bioassay of caffeine using sensor implant. Neuromolecular Medicine. 2009 Mar;11(1):20–27.

[8] Leung W, Chan CP, Rainer TH, Ip M, Cautherley GWH, Renneberg R. InfectCheck CRP barcode-style lateral flow assay for semi-quantitative detection of C-reactive protein in distinguishing between bacterial and viral infections. Journal of Immunological Methods. 2008 Jul;336(1):30–36.

[9] Hever N, Belkin S. A dual-color bacterial reporter strain for the detection of toxic and genotoxic effects. Engineering in Life Sciences. 2006 Jun;6(3):319–323.

[10] Vermeeren V. Towards label-free, real-time biosensors: A nanocrystalline diamond-based sensor platform for DNA- and immunosensors. [Phd in Biomedical Sciences]. Hasselt University; 2008.

[11] Grausova L, Bacakova L, Kromka A, Vanecek M, Rezek B, Lisa V. Molecular markers of adhesion, maturation and immune activation of human osteoblast-like MG 63 cells on nanocrystalline diamond films. Diamond and Related Materials. 2009 Mar;18(2-3):258–263.

[12] Ariano P, Giudice AL, Marcantoni A, Vittone E, Carbone E, Lovisolo D. A diamond-based biosensor for the recording of neuronal activity. Biosensors & Bioelectronics. 2009 Mar;24(7):2046–2050.

[13] Gajewski W, Achatz P, Williams OA, Haenen K, Bustarret E, Stutzmann M, et al. Electronic and optical properties of boron-doped nanocrystalline diamond films. Physical Review B. 2009;79(4).

[14] Schena M, Schalon D, Davis RW, Brown PO. Quantitative monitoring of gene expression patterns with a complementary DNA microarray. Science. 1995;270(5235):467–470.

[15] Yang WS, Auciello O, Butler J, Cai W, Carlisle J, Gerbi J, et al. DNA-modified nanocrystalline diamond thin-films as stable, biologically active substrates. Nature Materials. 2002 Dec;1(4):253–257.

[16] Peierls R. Bemerkungen uber umwandlungstemperaturen. Helvetica Physica Acta. 1934;7(81).

[17] Peierls RE. Quelques proprietes typique des corpes solide. Analles de l'Institute Henri Pointcare. 1935;5(177).

[18] Landau LD. Zur theorie der phasenumwandelungen II. Physicalische Zeitschrift der Sowjetunion. 1937;11(26).

[19] Iijima S. Helical Microtubules of graphite. Nature. 1991;354(56).

[20] Novoselov KS, Geim AK, Morozov S, Jiang D, Zhang Y, Dubonos S, et al. Electric field effect in atomically thin carbon films. Science. 2004 Oct;306(5696):666–669.

[21] Novoselov K, Jiang D, Schedin F, Booth T, Khotkevich V, Morozov S, et al. Two-dimensional atomic crystals. Proceedings of the National Academy of Sciences of the USA. 2005 Jul;102(30):10451–10453.

[22] Geim A, Novoselov K. The rise of graphene. Nature Materials. 2007 Mar;6(3):183–191.

[23] Malesevic A, Vitchev R, Schouteden K, Volodin A, Zhang L, Tendeloo GV, et al. Synthesis of few-layer graphene via microwave plasma-enhanced chemical vapour deposition. Nanotechnology. 2008 Jul;19(30).

[24] Zhang H, Kikuchi N, Kogure T, Kusano E. Growth of carbon with vertically aligned nanoscale flake structure in capacitively coupled rf glow discharge. Vacuum. 2008 Apr;82(8):754–759.

[25] Malesevic A, Vizireanu S, Kemps R, Vanhulsel A, Haesendonck CV, Dinescu G. Combined growth of carbon nanotubes and carbon nanowalls by plasma-enhanced chemical vapor deposition. Carbon. 2007 Dec;45(15):2932–2937.

[26] Kuochu, Hwang. Efficient cleavage of carbon graphene layers by oxidants. Journal of the Chemical Society. 1995;x(2):173–174.

[27] Yuan GD, Zhang WJ, Yang Y, Tang YB, Li YQ, Wang JX, et al. Graphene sheets via microwave chemical vapor deposition. Chemical Physics Letters. 2009;467(4-6):361–364.

[28] Blake P, Hill EW, Neto AHC, Novoselov KS, Jiang D, Yang R, et al. Making graphene visible. Applied Physics Letters. 2007 Aug;91(6).

[29] Gilje S, Han S, Wang M, Wang KL, Kaner RB. A chemical route to graphene for device applications. Nano Letters. 2007 Nov;7(11):3394–3398.

[30] Stankovich S, Dikin DA, Piner RD, Kohlhaas KA, Kleinhammes A, Jia Y, et al. Synthesis of graphene-based nanosheets via chemical reduction of exfoliated graphite oxide. Carbon. 2007 Jun;45(7):1558–1565.

[31] Kobayashi K, Tanimura M, Nakai H, Yoshimura A, Yoshimura H, Kojima K, et al. Nanographite domains in carbon nanowalls. Journal of Applied Physics. 2007 May;101(9).

[32] Kinchin GH. The electrical properties of graphite. Proceedings of the Royal Society of London: Series A, Mathematical and Physical Sciences. 1952;271(1128).

[33] Novoselov KS, Geim AK, Morozov SV, Jiang D, Katsnelson MI, Grigorieva IV, et al. Two-dimensional gas of massless Dirac fermions in graphene. Nature. 2005 Nov;438(7065):197–200.

[34] Zhang Y, Tan J, Stormer HL, Kim P. Experimental observasion of the quantum Hall effect and Berry's phase in graphene. Nature. 2005;438:197–200.

[35] Bolotin KI, Sikes KJ, Jiang Z, Klima M, Fudenberg G, Hone J, et al. Ultrahigh electron mobility in suspended graphene. Solid State Communications. 2008 Jun;146(9-10):351–355.

[36] Nesladek M, Bogdan A, Deferme W, Tranchanta N, Bergonzoa P. Charge transport in high mobilitynext term single crystal diamond. Diamond and Related Materials. 2008;17.

[37] Zhou SY, Gweon GH, Graf J, Fedorov AV, Spataru CD, Diehl RD, et al. First direct observation of Dirac fermions in graphite. Nature Physics. 2006 Sep;2(9):595–599.

[38] Katsnelson MI, Novoselov KS. Graphene: New bridge between condensed matter physics and quantum electrodynamics. Solid State Communications. 2007 Jul;143(1-2):3–13.

[39] Ferrari AC, Meyer JC, Scardaci V, Casiraghi C, Lazzeri M, Mauri F, et al. The raman fingerprint of graphene. Physical Review Letters. 2006;97.

[40] van der Pauw LJ. A method of measuring specific resistivity and Hall effect of discs of arbitrary shape. Philips Research Reports. 1958;13(1).

[41] Katz E, Willner I. Probing biomolecular interactions at conductive and semiconductive surfaces by impedance spectroscopy: Routes to impedimetric immunosensors, dna-sensors, and enzyme biosensors. Electroanalysis. 2003;15(11).

# Thesis Poster

universiteit hasselt

## Carbon Nanoflakes and Carbon Nanowalls: An Innovation in Biosensors

Matthias Van Gompel

*Instituut voor Materiaal Onderzoek*

universiteit hasselt INSTITUUT VOOR MATERIAALONDERZOEK

### Introduction

Over the last couple of years, graphene and other related materials such as carbon nanowalls (CNWs) and carbon nanoflakes (CNFs) have become a very important research subject in microelectronics. The use of these new carbon materials to develop a fast and sensitive biosensor is not yet explored. CNWs and CNFs with a thickness between two to ten graphene layers, exhibit special properties like ballistic electron transport, and very high mobilities, which can reach 200000 $cm^2 V^{-1} s^{-1}$. CNWs are biofunctionalized covalently with ssDNA and hybridization with complementary ssDNA is done. This ssDNA is labeled with alexa-488, to detect it with fluorescence microscopy. To test selectivity, hybridization is also performed with one mismatch DNA. The sensor setup was able to detect single point mutations in the DNA strands. To test the impedance of the CNFs, an array of interdigital gold electrodes is produced by using photolithography.

### CNW and CNF synthesis

The CNWs were produced by VITO using MW PECVD. In MW PECVD, an argon plasma is created under vacuum conditions, with a radio frequency plasma source. Methane and hydrogen are injected. The formed radicals attach to the substrate, forming CNWs. The CNFs are produced by using the method developed by A. V. Geim and K.S. Novoselov. Duct tape is used to cleave HOPG, and is pressed to a substrate. Small flakes are left behind on the glass or silicon substrate.

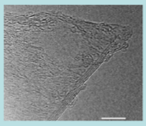

### Measurement techniques

To investigate covalent attachment on the CNWs, a first series of experiments is done with single stranded probe DNA, again labeled with alexa-488. The fluorescence is subsequently examined with a confocal fluorescence microscope, to be able to bleach the fluorescent label. The hybridization experiments are measured with a regular fluorescence microscope.

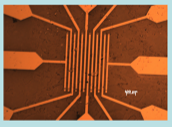

### Biofunctionalization

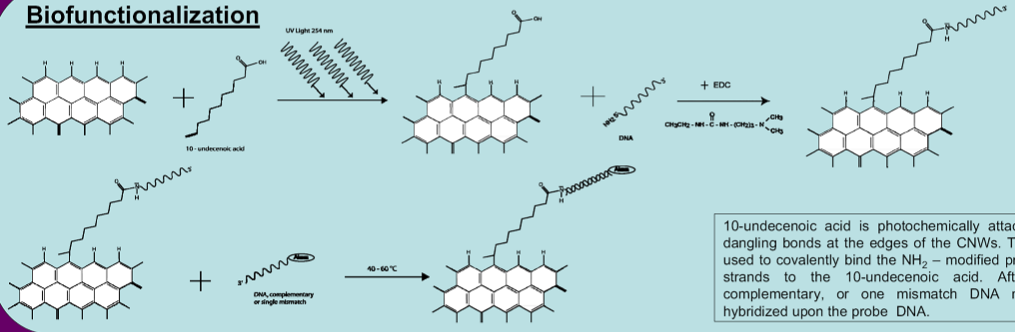


10-undecenoic acid is photochemically attached to the dangling bonds at the edges of the CNWs. Then EDC is used to covalently bind the $NH_2$ – modified probe ssDNA strands to the 10-undecenoic acid. After this, a complementary, or one mismatch DNA molecule is hybridized upon the probe DNA.

### Results

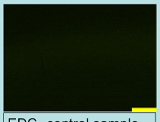

EDC- control sample. Complementary hybridization at 40°

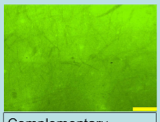

Complementary hybridization at 40°

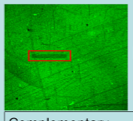

Complementary hybridization at 60°. The red rectangle indicates a bleached spot

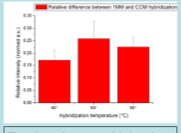

Testing the sensitivity, by comparing complementary and one mismatch ssDNA

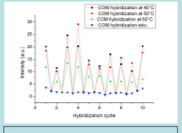

Testing the reusability of the sensor, and comparing hybridization temperatures

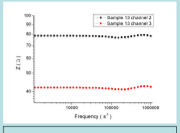

Impedance measurement of two CNFs

### Conclusion

When EDC- and EDC+ samples were compared, it was found that ssDNA can be covalently bonded to CNWs. Since hybridization with complementary or mismatch DNA was still possible, the biological activity of the DNA was preserved. The selectivity of hybridization was sensitive enough to clearly distinguish between complementary and one mismatch strands, making SNP detection possible. The sensor was able to do ten consecutive measurements, clearly showing reusability. The measured impedance of the CNFs is very low, thus showing great promise to develop a sensor, outperforming current ones in sensitivity.

# Publications and Posters

- R. Vansweevelt, A. Malesevic, M. Van Gompel, A. Vanhulsel, S. Wenmackers, V. Vermeeren, M. Ameloot, L. Michiels, C. Van Haesendonck and P. Wagner. "Biological modification of carbon nanowalls with ssDNA strands and subsequent hybridization experiments with fully complementary and mismatch DNA." In progress.

- Poster BPS 2009: R. Vansweevelt, A. Malesevic, M. Van Gompel, A. Vanhulsel, S. Wenmackers, V. Vermeeren, M. Ameloot, L. Michiels, C. Van Haesendonck and P. Wagner. "Biological modification of carbon nanowalls with ss-DNA and subsequent hybridization."

- Poster EnFI 2009: R. Vansweevelt, A. Malesevic, M. Van Gompel, A. Vanhulsel, S. Wenmackers, V. Vermeeren, M. Ameloot, L. Michiels, C. Van Haesendonck and P. Wagner. "Covalent DNA binding and hybridization experiments on carbon nanowall platforms."